Physiological Significance of R-fMRI Indices in Detecting Structural Brain Lesions

Zhen Fan[1], Xiao Chen[2,3], Zeng-Xin Qi[1], Le Li[2,4], Bin Lu[2,3], Cong-Lin Jiang[1], Ren-Qing Zhu[1], Liang Chen[1,*], Chao-Gan Yan[2,3,4,5,*]

Zhen Fan and Xiao Chen contributed equally to this work.

[1]Department of Neurosurgery, Huashan Hospital, Fudan University, Shanghai Neurosurgical Clinical Center, Shanghai, China; [2]CAS Key Laboratory of Behavioral Science, Institute of Psychology, Beijing, China; [3]Department of Psychology, University of Chinese Academy of Sciences, Beijing, China; [4]Magnetic Resonance Imaging Research Center, Institute of Psychology, Chinese Academy of Sciences, Beijing, China; [5]Department of Child and Adolescent Psychiatry, NYU Langone Medical Center School of Medicine, New York, NY, USA

***Corresponding authors:**

Chao-Gan Yan, Ph.D.

CAS Key Laboratory of Behavioral Science, Institute of Psychology, Beijing, China

16 Lincui Road, Chaoyang District, Beijing 100101, China

Tel: +86-10-64101582

Fax: +86-10-64101582

E-mail: ycg.yan@gmail.com

Correspondence may also be addressed to:

Liang Chen, Ph.D., M.D.

No. 12 Mid Wulumuqi Rd, Department of Neurosurgery, Hua Shan Hospital, Fudan University, Shanghai Neurosurgery Clinical Center, Shanghai 200040, P.R. China.

E-mail: chenlianghs@126.com

ABSTRACT

Resting-state functional MRI (R-fMRI) research has recently entered the era of “big data”, however, the physiological underpinnings of R-fMRI indices were rarely validated. Although studies have reported various neuropsychiatric disorders exhibit R-fMRI abnormalities, these “biomarkers” have not been validated in detecting structural lesions (brain tumors) as a concept proof. We enrolled 60 patients with intracranial tumors located in the unilateral cranial cavity and 60 matched normal controls to test whether R-fMRI indices can differentiate tumors. Common R-fMRI indices of tumors and the contralateral normal areas (for amplitude of low frequency fluctuations (ALFF), fractional ALFF (fALFF), regional homogeneity (ReHo) and degree centrality (DC)) and ipsilateral regions surrounding the tumors (for voxel-mirrored homotopic connectivity (VMHC)), were comprehensively assessed. According to paired *t*-tests, ReHo and DC failed in distinguishing tumors from their counterpart control regions in the cases without *Z*-standardization (subtracting the brain mean and dividing by the brain standard deviation (SD)). With *Z*-standardization, all measures can differentiate substantial tumors from normal neural regions in patients. To validate the lower power in the between-subject design than in the within-subject design, each metric was calculated in a matched control group, and two-sample *t*-tests were used to compare the patient tumors and the normal controls at the same area. ReHo and DC failed to detect significant differences between tumors and the sham tumors areas of normal controls, even with *Z*-standardization. This study tested the premise of R-fMRI biomarkers for detecting lesions and brings a new understanding to physical significance of the

Z-standardization.

KEYWORDS: Resting-state fMRI; Standardization; Biomarker; Cerebellum; Tumor

1. INTRODUCTION

Resting-state functional magnetic resonance imaging (R-fMRI) is one of the most rapidly expanding areas of neuroimaging research. As ease of data collection in diseased people, and amenability to aggregation across studies and sites, R-fMRI is particularly suitable for clinical applications (Biswal, et al., 2010; Castellanos, et al., 2013; Yan, et al., 2013b; Zuo and Xing, 2014). An increasing number of R-fMRI indices have been proposed to characterize clinical populations with various neuropsychiatric disorders (Craddock, et al., 2013; Zuo and Xing, 2014), and several of these indices have produced consistent and reliable results corresponding to functional areas within single individuals reliably (Castellanos, et al., 2013; Lang, et al., 2014). As we have entered an era of "Big Data", vast opportunities in R-fMRI research are available to take advantage of advanced data-intensive machine learning methodologies, such as deep learning along with open source computational platforms to discover validated biomarkers not only for diagnosis but also for assessing disease risk, prognosis and treatment response (Bzdok and Yeo, 2017; Kapur, et al., 2012; Xia and He, 2017). In particular, several promising R-fMRI biomarker studies have recently been reported (Abraham, et al., 2017; Drysdale, et al., 2017).

However, the physiological mechanisms underlying R-fMRI indices are still not well understood (Liu, 2013; Zhang and Raichle, 2010), although some evidence has been provided in the literature. First, the patterns of the networks defined by R-fMRI spontaneous fluctuations reflect the underlying organizational rules of the brain's anatomy (Baria, et al.,

2011). This fact was further validated by tract-tracing methods in the non-human primates (Kelly, et al., 2010; Margulies, et al., 2009). Second, a series of electrophysiological studies of the brains of humans, non-human primates, and other mammalians, particularly those employing intracranial electrodes, linked neural activity to ongoing fMRI fluctuations, especially using intracranial electrodes (Hacker, et al., 2017; He, et al., 2008; Keller, et al., 2011; Leopold and Maier, 2012; Liu, et al., 2011; Scholvinck, et al., 2013). Moreover, suggestive of validity in the R-fMRI have been linked to individual differences in behavior and pathology have suggested the validity of assessing R-fMRI fluctuations (Craddock, et al., 2013; Di Martino, et al., 2014). However, all this evidence only partially explains the underpinings of R-fMRI; the details remain unresolved, causing difficulty in interpreting changes in resting state activity and impeding the path of R-fMRI toward clinical applications.

Prior to further exploring the clinical value of R-fMRI indices, the presuppositions of whether common indices are able to detect obvious structural lesions (such as brain tumors) should be considered first. To date, most R-fMRI studies of brain tumors have focused on surgical planning to identify and located the eloquent areas in order to reduce the risk of postoperative functional deficits (Lang, et al., 2014; Pernet, et al., 2016; Qiu, et al., 2014; Zhang and Raichle, 2010). However, no study has explored the signals of tumors themselves, from the perspective of concept proof of R-fMRI indices in clinical applications. If an R-fMRI index cannot even detect obvious structural lesions, it likely cannot be trusted as a tool for studying diseases without structural lesions or, consequently, as a biomarker for further big data

studies. Thus, whether R-fMRI methodologies have the capacity for distinguishing pathological lesions from normal brain structures should be a fundamental prerequisite for further biomarker investigations.

To address these issues, we first comprehensively assessed common R-fMRI metrics of tumors and their counterpart control brain regions, which were defined as contralateral control areas to the tumors (for amplitude of low frequency fluctuations (ALFF), fractional ALFF (fALFF), regional homogeneity (ReHo) and degree centrality (DC)) and ipsilateral regions surrounding the tumors (for voxel-mirrored homotopic connectivity (VMHC)). We used paired t-tests to compare each measure between the tumor region and the counterpart control regions, respectively. Second, to validate the lower power in the between-subject design than in the within-subject design, each metric was calculated in a matched control group, and two-sample t-tests were used to compare the patient tumor areas with the same areas in the normal controls. Furthermore, we compared the measures with and without Z-standardization (subtracting the brain mean and dividing by the brain standard deviation (SD)) to explore the significance, as previous work demonstrated the importance of standardization (Yan, et al., 2013b). We hypothesized that (i) R-fMRI metrics can detect structural lesions (brain tumors), (ii) Z-standardization can enhance the validity of R-fMRI metrics, and that (iii) within-subject designs are superior to between-subject designs in identifying tumors.

2. MATERIALS AND METHODS

2.1. Subjects

A total of 60 patients with intracranial tumors, which located in the lateral posterior cranial fossa without spreading across the median to the contralateral side or obvious edema, were enrolled in this study (25 females; 21-72 years; 23 left side tumors). The pathological outcomes of these tumors were verified after operations and turned out to be the meningiomas, neurinomas, hemangioblastomas metastases and cholesteatomas. Of note, none of the tumors exhibited any neural activity whatsoever, and their original tissues did not contain any neurons. In addition, the edges of these tumors were clear, making them suitable for validating the physiological meaning underlying R-fMRI (Jiang, et al., 2010). Approval of this study was provided by the independent Ethics Committee of Huashan Hospital, Fudan University. Written informed consent was obtained from all subjects. Meanwhile, 60 sex-matched (p= 0.5812; t =0.5532) and age-matched (p = 0.5133; t = -0.6548) healthy individuals were included as the control group.

2.2. Imaging acquisition

All images were acquired using a Siemens Magnetom Verio 3.0 T MRI scanner (Siemens Medical Solutions, MAGNETOM, Germany). All patients were scanned preoperatively using R-fMRI (TR = 2,000 ms; TE = 35 ms; flip angle = 90°; slice number = 33; field of view [FOV] = 210 × 210 mm; voxel size = 3.3 × 3.3 × 4.0 mm^3). During the scanning, subjects were asked to remain still with their eyes closed. No task was given to the subjects, but they were told not

to fall asleep. Scans lasted for 8 minutes for a total of 240 time points per subject. Each run was preceded by 6-s dummy scans for magnetization stabilization. Additionally, high-resolution anatomical images were acquired with an axle magnetization-prepared rapid gradient echo T1-weighted sequence with contrasts (Gadopentetate Dimeglumine) (TR = 1900 ms; TE = 2.93 ms; flip angle = 90°; matrix size = 256 × 215; slice number = 176; slice thickness = 1 mm; FOV = 250 × 219 mm).

2.3. Preprocessing

All preprocessing was performed using the Data Processing Assistant for Resting-State fMRI (DPARSF, Yan and Zang, 2010, http://rfmri.org/DPARSF), which is based on Statistical Parametric Mapping (SPM, http://www.fil.ion.ucl.ac.uk/spm) and the toolbox for Data Processing & Analysis of Brain Imaging (DPABI, Yan, et al., 2016, http://rfmri.org/DPABI). First, the initial 10 volumes were discarded, and slice-timing correction was performed with all volume slices corrected for different signal acquisition times by shifting the signal measured in each slice relative to the acquisition of the slice at the midpoint of each TR. Then, the time series of images for each subject were realigned using a six-parameter (rigid body) linear transformation with a two-pass procedure (registered to the first image and then registered to the mean of the images after the first realignment). After realignment, individual T1-weighted MPRAGE images were co-registered to the mean functional image using a 6 degree-of-freedom linear transformation without re-sampling and then segmented into gray matter (GM), white matter (WM) and cerebrospinal fluid (CSF) (Ashburner and Friston, 2005).

Finally, transformations from the individual native space to the Montreal Neurological Institute (MNI) space were computed with the Diffeomorphic Anatomical Registration Through Exponentiated Lie algebra (DARTEL) tool (Ashburner, 2007).

2.4. Nuisance regression

To minimize head motion confounds, we utilized the Friston 24-parameter model (Friston, et al., 1996) to regress out head motion effects. The Friston 24-parameter model (which considers 6 head motion parameters, the 6 head motion parameters at the previous time point, and the 12 corresponding squared items) was chosen based on prior work indicating that higher-order models remove head motion effects better (Satterthwaite, et al., 2013; Yan, et al., 2013a). As global signal regression (GSR) is still a controversial practice in the R-fMRI field (Murphy and Fox, 2016), we examined the results without GSR but performed a validation with GSR in the supplementary analyses. Other sources of spurious variance (WM and CSF signals) were also removed from the data through linear regression to reduce respiratory and cardiac effects. Additionally, linear trends were included as a regressor to account for drifts in the blood oxygen level-dependent (BOLD) signal. We performed temporal bandpass filtering (0.01-0.1 Hz) on all time series except for ALFF and fALFF analyses.

2.5. A broad array of R-fMRI metrics

Amplitude of low frequency fluctuations (ALFF) (Zang, et al., 2007) and fractional ALFF (fALFF) (Zou, et al., 2008a): ALFF is the mean of amplitudes within a specific frequency domain (here, 0.01-0.1 Hz) from a fast Fourier transform of a voxel's time course. fALFF is a normalized version of ALFF and represents the relative contribution of specific oscillations to the whole detectable frequency range.

Regional homogeneity (ReHo) (Zang, et al., 2004): ReHo is a rank-based Kendall's coefficient of concordance (KCC) that assesses the synchronization among a given voxel and its nearest neighbors' (here, 26 voxels) time courses.

Degree centrality (DC) (Buckner, et al., 2009; Zuo, et al., 2012): DC is the number or sum of weights of significant connections for a voxel. Here, we calculated the weighted sum of positive correlations by requiring each connection's correlation coefficient to exceed a threshold of $r>0.25$ (Buckner, et al., 2009).

Voxel-mirrored homotopic connectivity (VMHC, Anderson, et al., 2011a; Zuo, et al., 2010b): VMHC corresponds to the functional connectivity between any pairs of symmetric inter-hemispheric voxels, that is, the Pearson's correlation coefficient between the time series of each voxel and that of its counterpart voxel at the same location in the opposite hemisphere. The resultant VMHC values were Fisher-Z transformed. For better correspondence between symmetric voxels, VMHC required that individual functional data be

further registered to a symmetric template and smoothed (4 mm FWHM). The group-averaged symmetric template was created by first computing a mean normalized T1 image across participants, and then this image was averaged with its left–right mirrored version (Zuo, et al., 2010b).

For further analyses, all of the metric maps were calculated with and without Z-standardization (subtracting the mean value for the entire brain from each voxel, and dividing by the corresponding SD) and then smoothed (4 mm FWHM), except for VMHC (which was smoothed beforehand and Fisher's r-to-z transformed).

2.6. Strategies to compare the indices of tumor regions with corresponding control areas

We manually drew the tumor's edge of each subject for use as the tumor masks using MRIcroN (http://people.cas.sc.edu/rorden/mricron/main.html). For ALFF, fALFF, ReHo and DC, corresponding control areas were defined as the normal symmetric inter-hemispheric voxels of the tumors. For the VMHC, corresponding control areas were defined at the tumors' periphery, which were derived by enlarging the tumors area by 4 voxels and subtracting the original tumor area, using a MATLAB-based script called y_MaskEnlarge (http://d.rnet.co/Programs_YAN/y_MaskEnlarge.m).

Each metric of the tumor mask and the corresponding control area was then averaged within the mask or the corresponding control area for the same subject, allowing us to perform group-level paired t-tests for the within-subject design.

To prove that a significant difference did not exist in the null conditions, 60 matched normal controls underwent the same analysis, considering the normal controls to have sham tumors at the same locations as the tumors in the patients, and comparing the five indices of the sham tumors with those of the corresponding sham control regions.

Moreover, to confirm the validity of the within-subject design, we compared each metric of the tumors in the patients with the sham tumors in the matched controls using two-sample t-tests, as the metrics in this case were derived from different subjects. This procedure allowed us to investigate differences between the within-subject design and the between-subject design.

3. RESULTS

3.1. Overlaps of tumor masks

A total of 60 intracranial tumors located in the unilateral posterior cranial fossa were identified, including 27 tumors located on the left side and 37 tumors on the right side. Tumor masks were defined according to the clear boundaries in high-resolution T1 images normalized to the MNI spaces using DPABI. The tumors overlap probabilistic images are depicted in Figure 1.

3.2. Comparison between Indices of tumor and corresponding control areas in the patient group

We first compared the means of each metric of the tumors and the corresponding control areas. For ALFF, fALFF, ReHo and DC, the corresponding control areas were defined as the tumors' symmetric inter-hemispheric voxels. For VMHC, the corresponding control areas were defined as the 4 voxels of the tumors periphery. Paired Student's *t*-tests were conducted to determine whether significant differences existed. Without Z-standardization, we found that the tumors' ALFF and fALFF were significantly different from those of the corresponding control areas ($p<0.05$), indicating the ability of these values to distinguish tumors from corresponding control areas (ALFF $p = 0.0008$, $t = -3.5230$; fALFF $p = 0.0081$, $t = -2.7399$). However, ReHo and DC failed to distinguish tumors from the corresponding control areas (ReHo, $p = 0.1178$, $t = -1.5875$; DC, $p = 0.4648$, $t = -0.7357$) (Table 1 and Figure 2). With *Z*-standardization, all the above indices were significantly differed between tumors and the corresponding control areas (ALFF $p =0.0001$, $t = -4.0888$; fALFF $p = 0.0237$, $t = -2.3218$; ReHo, $p= 0.0460$, $t = -2.0389$; DC, $p= 0.0000$, $t = -4.9362$). In contrast to the above 4 indices, VMHC was Fisher's r-to-z transformed (rather than Z-standardized) and compared with the surrounding control areas (rather than with inter-hemispheric areas).Using this method, VMHC successfully detected tumors ($p = 0.0000$, $t = -8.7502$) (Table 1 and Figure 2).

3.3. Comparison between indices of sham tumors and the corresponding sham control areas in the normal control group

To verify that the significant differences are not false positives (i.e., they do not exist in null conditions), we next compared the five indices of healthy controls' sham tumors with those of the corresponding sham control areas. Not surprisingly, all five indices were not significantly different between the sham tumors and the corresponding sham control areas (p>0.05) regardless of whether Z-standardization (not including VMHC) was employed (Table 1 and Figure 2). This result demonstrated that the normal neural activities of original tumors regions did not differ from those of the corresponding control regions, which verifies that the significant results described above for the patient group are not due to false positives.

3.4. Different profiles of R-fMRI indices in detecting tumors

After employing Z-standardization, ReHo and DC along with other common indices were able to detect tumors (Figure 2). To explore the different profiles of the five R-fMRI indices in detecting tumors, we converted the p values to z values to identify the differences between tumors and control areas (Figure 3). VMHC showed the greatest significant difference, followed by DC, ALFF and fALFF, successively. ReHo demonstrated the least significant difference (p = 0.046). In contrast, the p values of the five indices for the controls were all higher than 0.05 regardless of whether Z-standardization was employed.

3.5. Between-subject design decreased the power in differentiating tumors

To compare the power of the between-subject design with the within-subject design, we compared each metric of the tumors in the patient group with the metric of sham tumors in the matched control group using two samples t-tests, as different subjects were being compared. Before employing Z-standardization, only ALFF (p = 0.0183, t = -2.3933) could distinguish tumors from normal areas (Table 1). After employing Z-standardization in this between-subject design, ALFF and fALFF (ALFF p = 0.0029, t = -3.0441; fALFF p = 0.0412, t = -2.0641) were significantly different between the tumors in the patients and the sham tumors in the matched controls with this between-subject design. With Fisher's r-to-z transformation, VMHC again successfully detected tumors according to unpaired t-tests. However, ReHo (p = 0.0892, t = 1.7137) and DC (p = 0.4043, t = -0.837) (Table 1) failed to distinguish tumors from normal areas (Figure 4), even after employing Z-standardization.

4. DISCUSSION

With the development of new methodological strategies, particularly in the era of big data, R-fMRI research has shed light on clinical applications, such as the identification of new metrics that can serve as biomarkers for delineating and diagnosing novel subtypes of neurological diseases that are characterized by uniform neurobiological substrates (Abraham, et al., 2017; Bzdok and Yeo, 2017; Drysdale, et al., 2017; Xia and He, 2017). However, such applications depend on the understanding the physiological underpinnings of R-fMRI indices. The aim of this study was to test the ability of R-fMRI indices to differentiate brain tissues lacking neural signals from those with neural signals. Here, we comprehensively assessed

five common indices of R-fMRI indices for their ability to discriminate tumors from their counterpart control brain regions, and we compared the results regarding whether or not Z-standardization was employed, except for VMHC, which was Fisher's r-to-z transformed. Interestingly, only ALFF, fALFF and VMHC could successfully differentiate substantial tumors from normal neural regions (paired t-test, $p<0.05$). These corresponding regions did not show significant differences when compared within the normal controls (paired t-tests, $p>0.05$). Furthermore, ReHo and DC were not able to detect tumors unless Z-standardization was performed. To verify whether our primary analyses without GSR could be generalized to with GSR, we calculated the results with GSR and presented this analysis in the supplementary materials. ReHo and DC still could not significantly differentiate tumors significantly, and this persisted even when Z-standardization was employed (Table S1 and Figure S1). These findings suggest that GSR decreases, not increases, the ability of R-fMRI indices to detect tumors.

4.1. Utilities of common R-fMRI metrics in detecting structural lesions

Previous studies have suggested that low-frequency (typically 0.01-0.1 Hz) oscillations (LFO) are related to metabolic correlations of neuronal activity. Researchers have explored the amplitude of BOLD signals in healthy populations and found that ALFF exhibits significant differences among different brain tissues (e.g., GM and WM) (Biswal, et al., 1995), different brain regions (e.g., visual and auditory regions), and different physiological states (e.g., eyes closed vs. eyes open) (Yan, et al., 2009; Yang, et al., 2007). Several research groups have

also discovered abnormal ALFF in brain disorders, such as in attention-deficit/hyperactivity disorder (Zang, et al., 2007), Alzheimer's disease (AD) (He, et al., 2007), schizophrenia (Hoptman, et al., 2012; Turner, et al., 2012; Turner, et al., 2013; Yu, et al., 2014), mild cognitive impairment (Han, et al., 2011), Parkinson's disease (PD) (Hou, et al., 2014), and refractory temporal lobe epilepsy (Ji, et al., 2014; Zhang, et al., 2010).

Fractional ALFF (fALFF) approach was defined as the ratio of the low-frequency power spectrum (0.01–0.1 Hz) to the power spectrum of the entire detectable frequency range. As a normalized index of ALFF, fALFF can provide a more specific measure of low-frequency oscillatory phenomena and selectively suppress artifacts from non-specific brain areas; in addition, it can enhances signals from cortical regions associated with brain activity and makes use of the distinct characteristics of their signals in the frequency domain (He, et al., 2007; Zuo, et al., 2010a). fALFF is generally more effective in analyzing both healthy people and individuals with brain abnormalities, particularly in the perivascular, periventricular and periaqueductal regions. When applied to brains with a pathological structure, both ALFF and fALFF had lower values within the tumor masks than in the counterpart regions, making them able to distinguish tumors from normal regions. Such results offered sort of sufficient proofs to verify they were suggestive for regional spontaneous neuronal activity, which have been demonstrated in previous researches (Han, et al., 2011; He, et al., 2007; Hou, et al., 2014; Qian, et al., 2015; Yu, et al., 2014; Zang, et al., 2007; Zou, et al., 2008b).

ReHo, which represents the KCC between a given voxel's time-series and its 26 adjacent neighbors, detected voxels that were more temporally homogeneous within a functional brain area when the area was involved in a specific condition (Zang, et al., 2004). ReHo serves as an R-fMRI metric for investigating neural activities in normal brain networks and clinical features in several diseases, such as AD (Liu, et al., 2008; Zhang, et al., 2012), PD (Wu, et al., 2009), epilepsy (Zhong, et al., 2011) and psychiatric disorders (Dichter, et al., 2015; Dutta, et al., 2014; Paakki, et al., 2010; Peng, et al., 2014; Yuan, et al., 2008), and it reflects stable trait properties (Zuo, et al., 2013). Although a robust R-fMRI metric with high test-retest reliability (Zuo and Xing, 2014), ReHo failed to detect tumors in this study unless Z-standardization was utilized. One reasonable explanation is that tumors have the blood supplies and do not display fluctuations as normal neural activities do, which causes tumors to mimic the homogeneous sham situation to some extent. However, after the suppressing of confounding factors by Z-standardization, ReHo could differentiate tumors from control areas. This result emphasizes the fact that R-fMRI signals are derived from the hemodynamic reactions and the importance of considering physiological noise in R-fMRI studies.

Extensive evidence suggests that some brain areas act as hubs that are distinctively interconnected distinctively, functionally specialized systems. However, these hubs are susceptible to disconnection and dysfunction in certain brain disorders (Buckner, et al., 2009; Zuo, et al., 2012). DC is the number or sum of weights of significant connections for a voxel. As such, centrality measures allow us to capture the complexity of the functional networks as

a whole. We calculated the weighted sum of positive correlations by requiring each connection's correlation coefficient to exceed a threshold of r>0.25 (Buckner, et al., 2009). Unfortunately, DC could not discriminate tumors from corresponding control areas in our study unless standardization was employed. This fact implies that DC has its limitations. The degree that hubs reflecting activity fluctuations driven by local projections compared with distant projections remains unclear. Our observations indicated that DC failed to elaborate local activities. Furthermore, DC was a low test-retest reliabilitiy measure (Zuo and Xing, 2014), and GSR had substantial influence on its spatial pattern (Liao, et al., 2013; Murphy and Fox, 2016). This study highlights the importance of employing Z-standardization rather than GSR when exploring functional networks using DC, not only because its test-retest reliability improved without GSR (Liao, et al., 2013), but also because DC with Z-standardization employed had the ability to detect structural lesions.

The high degree of synchrony in spontaneous activity between geometrically corresponding inter-hemispheric regions is a fundamental characteristic of the intrinsic functional architecture of the brain. (VMHC, Anderson, et al., 2011a; Zuo, et al., 2010b) represents a useful screening method for evaluating neurological disorders where neural connectivity is implicated in the pathophysiology, such as in autism (Anderson, et al., 2011b), schizophrenia (Hoptman, et al., 2012), seizures (Ji, et al., 2014) and AD (Dai, et al., 2015). Our study revealed a consistent result, as VMHC was the most reliable measure in detecting structural lesions, proving that it is a credible measure to explore intrinsic network architecture.

4.2. The significance of Z-standardization

Remarkable site-related variations along with a multitude of experimental, environmental and subject-related factors further challenge R-fMRI measures, especially given that R-fMRI research has entered the era of “big data” (Bzdok and Yeo, 2017; Xia and He, 2017; Yan, et al., 2013b). Big data from multiple centers play a practical role in clinical applications, particularly holding promise for use in validating biomarkers with the assistance of advanced data-intensive machine learning methodologies, such as deep learning (Arbabshirani, et al., 2017). A recent, intriguing study using R-fMRI data from 1200 subjects offered an impressive example in which subtypes of depression could be defined by R-fMRI data (Drysdale, et al., 2017). Another connectome-based study reported the prediction of biomarkers study in autism patients using big data (Abraham, et al., 2017). However, with new advances come new challenges. Big data also provides a stark portrayal of variability in imaging methodologies employed in the neuroimaging field (Teipel, et al., 2017; Wald and Polimeni, 2017). Big Data can be easily polluted by noise due to the aggregation of data collected via different research designs and data collection methods, particularly imaging sites (Xia and He, 2017), which emphasizes the need to establish consistent acquisition protocols, relevant equipment and software throughout studies. Unfortunately, standardizing all of these factors across studies is not always feasible. Although studies have highlighted the utility of post-acquisition standardization techniques in minimizing the influences of nuisance variables on inter-individual variation (Yan, et al., 2013b), less is known regarding the validity

of such techniques in lesion detection. ReHo and DC failed to detect tumors unless Z-standardization was performed. Employing Z-standardization was effective in reducing nuisance effects and increasing test-retest reliability, allowing ReHo and DC to succeeded in detecting tumors. As a post-hoc standardization strategy was used widely, this study offers a new understanding of the substantial necessity of Z-standardization in era of big data.

4.3. Within-subject designs are crucial for R-fMRI research

Within-subject designs have gained popularity for their ability to decrease participant-related nuisance variations and increase power. Researchers generally prefer within-subject designs to between-subject designs where possible, as larger effect sizes in within-subject designs can increase reproducibility in small-sample-size studies (Chen, et al., 2018; Mumford, et al., 2014). This study emphasized the importance of within-subject designs again, as some R-fMRI indices, namely, ReHo and DC, could not detect tumors when calculated using the between-subject design, which compared the R-fMRI metrics of tumors with sham tumors in controls using two-sample *t*-test, even after employing Z-standardization. This result is in contrast to the within-subject design, for which all 5 R-fMRI indices were able to distinguish tumors from normal brain regions with Z-standardization. Therefore, researchers should prioritize within-subject designs over between-subject designs whenever possible.

4.4. Limitations and future directions

This study is characterized by several limitations. First, we only used cerebellar tumors to test the validity if R-fMRI indices in detecting lesions. This is because cerebellar asymmetry is weaker than cerebral asymmetry from a structural (Ito, 1984) and functional perspective (Wang, et al., 2013). Furthermore, the cerebellum contains nearly 4 times more neurons than the cerebral cortex but has a much smaller volume, and thus, cerebellar tumors caused less anatomic distortions in spatial normalization. Second, we only explored the differences in R-fMRI metrics between tumors and normal areas, although we did not compare their performances with other multi-modal MRI sequences. We plan to study the relations between R-fMRI and perfusion MRI, cerebral blood flow, and even intraoperative electrophysiological results in the futures, aiming to provide more evidence regarding the physiological underpinnings of R-fMRI. Third, a larger sample size would give us the opportunity to study on different tumor pathological types, which may provide new insight into ability of R-fMRI metrics to detect hypervascular tumors and hypovascular tumors. These limitations summarize additional aspects that we plan to explore in the future.

CONCLUSIONS

To the best of our knowledge, this is the first study to comprehensively evaluate the ability of different R-fMRI metrics to differentiate structural lesions, which should be the premise of identifying R-fMRI biomarkers in neuropsychiatric disorders. ALFF, fALFF and VMHC were able to discriminate tumors from normal regions, while ReHo and DC failed to detect structural lesions (brain tumors) unless Z-standardization was employed. These results

validated the implicit assumptions from the perspective of neurosurgeon that R-fMRI signals represented neural activity rather than noise. Furthermore, we recommend within-subject designs over between-subject designs whenever possible.

ACKNOWLEDGEMENTS

This work was supported by the National Key R&D Program of China (2017YFC1309902), the National Natural Science Foundation of China (81671774 and 81630031), the Hundred Talents Program of the Chinese Academy of Sciences, and Beijing Municipal Science & Technology Commission (Z161100000216152), Natural science foundation and major basic research program of shanghai (16JC1420100). The authors would like to thank Zhong Yang for assembling the image database.

CONFLICT OF INTEREST

The authors declare no competing financial interests.

REFERENCES

Abraham, A., Milham, M.P., Di Martino, A., Craddock, R.C., Samaras, D., Thirion, B., Varoquaux, G. (2017) Deriving reproducible biomarkers from multi-site resting-state data: An Autism-based example. Neuroimage, 147:736-745.

Anderson, J.S., Druzgal, T.J., Froehlich, A., DuBray, M.B., Lange, N., Alexander, A.L., Abildskov, T., Nielsen, J.A., Cariello, A.N., Cooperrider, J.R., Bigler, E.D., Lainhart, J.E. (2011a) Decreased interhemispheric functional connectivity in autism. Cerebral cortex, 21:1134-46.

Anderson, J.S., Druzgal, T.J., Froehlich, A., DuBray, M.B., Lange, N., Alexander, A.L., Abildskov, T., Nielsen, J.A., Cariello, A.N., Cooperrider, J.R., Bigler, E.D., Lainhart, J.E. (2011b) Decreased interhemispheric functional connectivity in autism. Cereb Cortex, 21:1134-46.

Arbabshirani, M.R., Plis, S., Sui, J., Calhoun, V.D. (2017) Single subject prediction of brain disorders in neuroimaging: Promises and pitfalls. Neuroimage, 145:137-165.

Ashburner, J. (2007) A fast diffeomorphic image registration algorithm. NeuroImage, 38:95-113.

Ashburner, J., Friston, K.J. (2005) Unified segmentation. NeuroImage, 26:839-851.

Baria, A.T., Baliki, M.N., Parrish, T., Apkarian, A.V. (2011) Anatomical and functional assemblies of brain BOLD oscillations. J Neurosci, 31:7910-9.

Biswal, B., Zerrin Yetkin, F., Haughton, V.M., Hyde, J.S. (1995) Functional connectivity in the motor cortex of resting human brain using echo-planar mri. Magnetic Resonance in Medicine, 34:537-541.

Biswal, B.B., Mennes, M., Zuo, X.-N., Gohel, S., Kelly, C., Smith, S.M., Beckmann, C.F., Adelstein, J.S., Buckner, R.L., Colcombe, S., Dogonowski, A.-M., Ernst, M., Fair, D., Hampson, M., Hoptman, M.J., Hyde, J.S., Kiviniemi, V.J., Kötter, R., Li, S.-J., Lin, C.-P., Lowe, M.J., Mackay, C., Madden, D.J., Madsen, K.H., Margulies, D.S., Mayberg, H.S., McMahon, K., Monk, C.S., Mostofsky, S.H., Nagel, B.J., Pekar, J.J., Peltier, S.J., Petersen, S.E., Riedl, V., Rombouts, S.A.R.B., Rypma, B., Schlaggar, B.L., Schmidt, S., Seidler, R.D., Siegle, G.J., Sorg, C., Teng, G.-J., Veijola, J., Villringer, A., Walter, M., Wang, L., Weng, X.-C., Whitfield-Gabrieli, S., Williamson, P., Windischberger, C., Zang, Y.-F., Zhang, H.-Y., Castellanos, F.X., Milham, M.P. (2010) Toward discovery science of human brain function. Proceedings of the National Academy of Sciences, 107:4734-4739.

Buckner, R.L., Sepulcre, J., Talukdar, T., Krienen, F.M., Liu, H., Hedden, T., Andrews-Hanna, J.R., Sperling, R.A., Johnson, K.A. (2009) Cortical hubs revealed by intrinsic functional connectivity: mapping, assessment of stability, and relation to Alzheimer's disease. J Neurosci, 29:1860-73.

Bzdok, D., Yeo, B.T.T. (2017) Inference in the age of big data: Future perspectives on neuroscience. NeuroImage, 155:549-564.

Castellanos, F.X., Di Martino, A., Craddock, R.C., Mehta, A.D., Milham, M.P. (2013) Clinical applications of the functional connectome. NeuroImage, 80:527-540.

Chen, X., Lu, B., Yan, C.-G. (2018) Reproducibility of R-fMRI metrics on the impact of different strategies for multiple comparison correction and sample sizes. Human Brain Mapping, 39:300-318.

Craddock, R.C., Jbabdi, S., Yan, C.-G., Vogelstein, J.T., Castellanos, F.X., Di Martino, A., Kelly, C., Heberlein, K., Colcombe, S., Milham, M.P. (2013) Imaging human connectomes at the macroscale. Nature Methods, 10:524.

Dai, Z., Yan, C., Li, K., Wang, Z., Wang, J., Cao, M., Lin, Q., Shu, N., Xia, M., Bi, Y., He, Y. (2015) Identifying and Mapping Connectivity Patterns of Brain Network Hubs in Alzheimer's Disease. Cerebral Cortex,

25:3723-3742.

Di Martino, A., Yan, C.G., Li, Q., Denio, E., Castellanos, F.X., Alaerts, K., Anderson, J.S., Assaf, M., Bookheimer, S.Y., Dapretto, M., Deen, B., Delmonte, S., Dinstein, I., Ertl-Wagner, B., Fair, D.A., Gallagher, L., Kennedy, D.P., Keown, C.L., Keysers, C., Lainhart, J.E., Lord, C., Luna, B., Menon, V., Minshew, N.J., Monk, C.S., Mueller, S., Muller, R.A., Nebel, M.B., Nigg, J.T., O'Hearn, K., Pelphrey, K.A., Peltier, S.J., Rudie, J.D., Sunaert, S., Thioux, M., Tyszka, J.M., Uddin, L.Q., Verhoeven, J.S., Wenderoth, N., Wiggins, J.L., Mostofsky, S.H., Milham, M.P. (2014) The autism brain imaging data exchange: towards a large-scale evaluation of the intrinsic brain architecture in autism. Mol Psychiatry, 19:659-67.

Dichter, G.S., Gibbs, D., Smoski, M.J. (2015) A systematic review of relations between resting-state functional-MRI and treatment response in major depressive disorder. Journal of Affective Disorders, 172:8-17.

Drysdale, A.T., Grosenick, L., Downar, J., Dunlop, K., Mansouri, F., Meng, Y., Fetcho, R.N., Zebley, B., Oathes, D.J., Etkin, A., Schatzberg, A.F., Sudheimer, K., Keller, J., Mayberg, H.S., Gunning, F.M., Alexopoulos, G.S., Fox, M.D., Pascual-Leone, A., Voss, H.U., Casey, B.J., Dubin, M.J., Liston, C. (2017) Resting-state connectivity biomarkers define neurophysiological subtypes of depression. Nat Med, 23:28-38.

Dutta, A., McKie, S., Deakin, J.F.W. (2014) Resting state networks in major depressive disorder. Psychiatry Research: Neuroimaging, 224:139-151.

Friston, K.J., Williams, S., Howard, R., Frackowiak, R.S.J., Turner, R. (1996) Movement-Related effects in fMRI time-series. Magn Reson Med, 35:346-355.

Hacker, C.D., Snyder, A.Z., Pahwa, M., Corbetta, M., Leuthardt, E.C. (2017) Frequency-specific electrophysiologic correlates of resting state fMRI networks. Neuroimage, 149:446-457.

Han, Y., Wang, J., Zhao, Z., Min, B., Lu, J., Li, K., He, Y., Jia, J. (2011) Frequency-dependent changes in the amplitude of low-frequency fluctuations in amnestic mild cognitive impairment: a resting-state fMRI study. Neuroimage, 55:287-95.

He, B.J., Snyder, A.Z., Zempel, J.M., Smyth, M.D., Raichle, M.E. (2008) Electrophysiological correlates of the brain's intrinsic large-scale functional architecture. Proceedings of the National Academy of Sciences, 105:16039-16044.

He, Y., Wang, L., Zang, Y., Tian, L., Zhang, X., Li, K., Jiang, T. (2007) Regional coherence changes in the early stages of Alzheimer's disease: a combined structural and resting-state functional MRI study. Neuroimage, 35:488-500.

Hoptman, M.J., Zuo, X.N., D'Angelo, D., Mauro, C.J., Butler, P.D., Milham, M.P., Javitt, D.C. (2012) Decreased interhemispheric coordination in schizophrenia: a resting state fMRI study. Schizophr Res, 141:1-7.

Hou, Y., Wu, X., Hallett, M., Chan, P., Wu, T. (2014) Frequency-dependent neural activity in Parkinson's disease. Hum Brain Mapp, 35:5815-33.

Ito, M. (1984) The Cerebellum and Neural. Control.

Ji, G.-J., Zhang, Z., Xu, Q., Zang, Y.-F., Liao, W., Lu, G. (2014) Generalized Tonic-Clonic Seizures: Aberrant Interhemispheric Functional and Anatomical Connectivity. Radiology, 271:839-847.

Jiang, Z., Krainik, A., David, O., Salon, C., Troprès, I., Hoffmann, D., Pannetier, N., Barbier, E.L., Bombìn, E.R., Warnking, J., Pasteris, C., Chabardes, S., Berger, F., Grand, S., Segebarth, C., Gay, E., Le Bas,

J.-F. (2010) Impaired fMRI activation in patients with primary brain tumors. NeuroImage, 52:538-548.

Kapur, S., Phillips, A.G., Insel, T.R. (2012) Why has it taken so long for biological psychiatry to develop clinical tests and what to do about it? Mol Psychiatry, 17:1174-9.

Keller, C.J., Bickel, S., Entz, L., Ulbert, I., Milham, M.P., Kelly, C., Mehta, A.D. (2011) Intrinsic functional architecture predicts electrically evoked responses in the human brain. Proceedings of the National Academy of Sciences, 108:10308-10313.

Kelly, C., Uddin, L.Q., Shehzad, Z., Margulies, D.S., Castellanos, F.X., Milham, M.P., Petrides, M. (2010) Broca's region: linking human brain functional connectivity data and non-human primate tracing anatomy studies. European Journal of Neuroscience, 32:383-398.

Lang, S., Duncan, N., Northoff, G. (2014) Resting-state functional magnetic resonance imaging: review of neurosurgical applications. Neurosurgery, 74:453-64; discussion 464-5.

Leopold, D.A., Maier, A. (2012) Ongoing physiological processes in the cerebral cortex. Neuroimage, 62:2190-200.

Liao, X.H., Xia, M.R., Xu, T., Dai, Z.J., Cao, X.Y., Niu, H.J., Zuo, X.N., Zang, Y.F., He, Y. (2013) Functional brain hubs and their test-retest reliability: a multiband resting-state functional MRI study. Neuroimage, 83:969-82.

Liu, T.T. (2013) Neurovascular factors in resting-state functional MRI. Neuroimage, 80:339-48.

Liu, X., Zhu, X.H., Zhang, Y., Chen, W. (2011) Neural origin of spontaneous hemodynamic fluctuations in rats under burst-suppression anesthesia condition. Cereb Cortex, 21:374-84.

Liu, Y., Wang, K., Yu, C., He, Y., Zhou, Y., Liang, M., Wang, L., Jiang, T. (2008) Regional homogeneity, functional connectivity and imaging markers of Alzheimer's disease: A review of resting-state fMRI studies. Neuropsychologia, 46:1648-1656.

Margulies, D.S., Vincent, J.L., Kelly, C., Lohmann, G., Uddin, L.Q., Biswal, B.B., Villringer, A., Castellanos, F.X., Milham, M.P., Petrides, M. (2009) Precuneus shares intrinsic functional architecture in humans and monkeys. Proceedings of the National Academy of Sciences, 106:20069-20074.

Mumford, J.A., Davis, T., Poldrack, R.A. (2014) The impact of study design on pattern estimation for single-trial multivariate pattern analysis. NeuroImage, 103:130-138.

Murphy, K., Fox, M.D. (2016) Towards a Consensus Regarding Global Signal Regression for Resting State Functional Connectivity MRI. Neuroimage.

Paakki, J.-J., Rahko, J., Long, X., Moilanen, I., Tervonen, O., Nikkinen, J., Starck, T., Remes, J., Hurtig, T., Haapsamo, H., Jussila, K., Kuusikko-Gauffin, S., Mattila, M.-L., Zang, Y., Kiviniemi, V. (2010) Alterations in regional homogeneity of resting-state brain activity in autism spectrum disorders. Brain Research, 1321:169-179.

Peng, D.-C., Dai, X.-J., Gong, H.-H., Li, H.-J., Nie, X., Zhang, W. (2014) Altered intrinsic regional brain activity in male patients with severe obstructive sleep apnea: a resting-state functional magnetic resonance imaging study. Neuropsychiatric Disease and Treatment, 10:1819-1826.

Pernet, C.R., Gorgolewski, K.J., Job, D., Rodriguez, D., Whittle, I., Wardlaw, J. (2016) A structural and functional magnetic resonance imaging dataset of brain tumour patients. Sci Data, 3:160003.

Qian, L., Zhang, Y., Zheng, L., Shang, Y., Gao, J.H., Liu, Y. (2015) Frequency dependent topological patterns of resting-state brain networks. PLoS One, 10:e0124681.

Qiu, T.M., Yan, C.G., Tang, W.J., Wu, J.S., Zhuang, D.X., Yao, C.J., Lu, J.F., Zhu, F.P., Mao, Y., Zhou, L.F. (2014) Localizing hand motor area using resting-state fMRI: validated with direct cortical stimulation.

Acta Neurochir (Wien), 156:2295-302.

Satterthwaite, T.D., Elliott, M.A., Gerraty, R.T., Ruparel, K., Loughead, J., Calkins, M.E., Eickhoff, S.B., Hakonarson, H., Gur, R.C., Gur, R.E., Wolf, D.H. (2013) An improved framework for confound regression and filtering for control of motion artifact in the preprocessing of resting-state functional connectivity data. Neuroimage, 64:240-56.

Scholvinck, M.L., Leopold, D.A., Brookes, M.J., Khader, P.H. (2013) The contribution of electrophysiology to functional connectivity mapping. Neuroimage, 80:297-306.

Teipel, S.J., Wohlert, A., Metzger, C., Grimmer, T., Sorg, C., Ewers, M., Meisenzahl, E., Kloppel, S., Borchardt, V., Grothe, M.J., Walter, M., Dyrba, M. (2017) Multicenter stability of resting state fMRI in the detection of Alzheimer's disease and amnestic MCI. Neuroimage Clin, 14:183-194.

Turner, J.A., Chen, H., Mathalon, D.H., Allen, E.A., Mayer, A.R., Abbott, C.C., Calhoun, V.D., Bustillo, J. (2012) Reliability of the amplitude of low-frequency fluctuations in resting state fMRI in chronic schizophrenia. Psychiatry Res, 201:253-5.

Turner, J.A., Damaraju, E., van Erp, T.G., Mathalon, D.H., Ford, J.M., Voyvodic, J., Mueller, B.A., Belger, A., Bustillo, J., McEwen, S., Potkin, S.G., Fbirn, Calhoun, V.D. (2013) A multi-site resting state fMRI study on the amplitude of low frequency fluctuations in schizophrenia. Front Neurosci, 7:137.

Wald, L.L., Polimeni, J.R. (2017) Impacting the effect of fMRI noise through hardware and acquisition choices - Implications for controlling false positive rates. Neuroimage, 154:15-22.

Wang, D., Buckner, R.L., Liu, H. (2013) Cerebellar asymmetry and its relation to cerebral asymmetry estimated by intrinsic functional connectivity. J Neurophysiol, 109:46-57.

Wu, T., Long, X., Zang, Y., Wang, L., Hallett, M., Li, K., Chan, P. (2009) Regional homogeneity changes in patients with Parkinson's disease. Human brain mapping, 30:1502-1510.

Xia, M., He, Y. (2017) Functional connectomics from a "big data" perspective. Neuroimage.

Yan, C., Liu, D., He, Y., Zou, Q., Zhu, C., Zuo, X., Long, X., Zang, Y. (2009) Spontaneous brain activity in the default mode network is sensitive to different resting-state conditions with limited cognitive load. PLoS One, 4:e5743.

Yan, C.-G., Cheung, B., Kelly, C., Colcombe, S., Craddock, R.C., Di Martino, A., Li, Q., Zuo, X.-N., Castellanos, F.X., Milham, M.P. (2013a) A comprehensive assessment of regional variation in the impact of head micromovements on functional connectomics. NeuroImage, 76:183-201.

Yan, C.G., Craddock, R.C., Zuo, X.N., Zang, Y.F., Milham, M.P. (2013b) Standardizing the intrinsic brain: towards robust measurement of inter-individual variation in 1000 functional connectomes. Neuroimage, 80:246-62.

Yan, C.G., Wang, X.D., Zuo, X.N., Zang, Y.F. (2016) DPABI: Data Processing & Analysis for (Resting-State) Brain Imaging. Neuroinformatics, 14:339-51.

Yan, C.G., Zang, Y.F. (2010) DPARSF: A MATLAB Toolbox for "Pipeline" Data Analysis of Resting-State fMRI. Front Syst Neurosci, 4:13.

Yang, H., Long, X.Y., Yang, Y., Yan, H., Zhu, C.Z., Zhou, X.P., Zang, Y.F., Gong, Q.Y. (2007) Amplitude of low frequency fluctuation within visual areas revealed by resting-state functional MRI. Neuroimage, 36:144-52.

Yu, R., Chien, Y.L., Wang, H.L., Liu, C.M., Liu, C.C., Hwang, T.J., Hsieh, M.H., Hwu, H.G., Tseng, W.Y. (2014) Frequency-specific alternations in the amplitude of low-frequency fluctuations in schizophrenia. Hum Brain Mapp, 35:627-37.

Yuan, Y., Zhang, Z., Bai, F., Yu, H., Shi, Y., Qian, Y., Liu, W., You, J., Zhang, X., Liu, Z. (2008) Abnormal neural activity in the patients with remitted geriatric depression: A resting-state functional magnetic resonance imaging study. Journal of Affective Disorders, 111:145-152.

Zang, Y., Jiang, T., Lu, Y., He, Y., Tian, L. (2004) Regional homogeneity approach to fMRI data analysis. NeuroImage, 22:394-400.

Zang, Y.F., He, Y., Zhu, C.Z., Cao, Q.J., Sui, M.Q., Liang, M., Tian, L.X., Jiang, T.Z., Wang, Y.F. (2007) Altered baseline brain activity in children with ADHD revealed by resting-state functional MRI. Brain Dev, 29:83-91.

Zhang, D., Raichle, M.E. (2010) Disease and the brain's dark energy. Nat Rev Neurol, 6:15-28.

Zhang, Z., Liu, Y., Jiang, T., Zhou, B., An, N., Dai, H., Wang, P., Niu, Y., Wang, L., Zhang, X. (2012) Altered spontaneous activity in Alzheimer's disease and mild cognitive impairment revealed by Regional Homogeneity. NeuroImage, 59:1429-1440.

Zhang, Z., Lu, G., Zhong, Y., Tan, Q., Liao, W., Wang, Z., Wang, Z., Li, K., Chen, H., Liu, Y. (2010) Altered spontaneous neuronal activity of the default-mode network in mesial temporal lobe epilepsy. Brain Research, 1323:152-160.

Zhong, Y., Lu, G., Zhang, Z., Jiao, Q., Li, K., Liu, Y. (2011) Altered regional synchronization in epileptic patients with generalized tonic–clonic seizures. Epilepsy Research, 97:83-91.

Zou, Q.-H., Zhu, C.-Z., Yang, Y., Zuo, X.-N., Long, X.-Y., Cao, Q.-J., Wang, Y.-F., Zang, Y.-F. (2008a) An improved approach to detection of amplitude of low-frequency fluctuation (ALFF) for resting-state fMRI: Fractional ALFF. J Neurosci Methods, 172:137-141.

Zou, Q.H., Zhu, C.Z., Yang, Y., Zuo, X.N., Long, X.Y., Cao, Q.J., Wang, Y.F., Zang, Y.F. (2008b) An improved approach to detection of amplitude of low-frequency fluctuation (ALFF) for resting-state fMRI: fractional ALFF. J Neurosci Methods, 172:137-41.

Zuo, X.-N., Xing, X.-X. (2014) Test-retest reliabilities of resting-state FMRI measurements in human brain functional connectomics: A systems neuroscience perspective. Neuroscience & Biobehavioral Reviews, 45:100-118.

Zuo, X.N., Di Martino, A., Kelly, C., Shehzad, Z.E., Gee, D.G., Klein, D.F., Castellanos, F.X., Biswal, B.B., Milham, M.P. (2010a) The oscillating brain: complex and reliable. Neuroimage, 49:1432-45.

Zuo, X.N., Ehmke, R., Mennes, M., Imperati, D., Castellanos, F.X., Sporns, O., Milham, M.P. (2012) Network Centrality in the Human Functional Connectome. Cereb Cortex, 22:1862-75.

Zuo, X.N., Kelly, C., Di Martino, A., Mennes, M., Margulies, D.S., Bangaru, S., Grzadzinski, R., Evans, A.C., Zang, Y.F., Castellanos, F.X., Milham, M.P. (2010b) Growing together and growing apart: regional and sex differences in the lifespan developmental trajectories of functional homotopy. J Neurosci, 30:15034-43.

Zuo, X.N., Xu, T., Jiang, L., Yang, Z., Cao, X.Y., He, Y., Zang, Y.F., Castellanos, F.X., Milham, M.P. (2013) Toward reliable characterization of functional homogeneity in the human brain: preprocessing, scan duration, imaging resolution and computational space. Neuroimage, 65:374-86.

TABLES

Table 1. Statistical results and significance levels of common R-fMRI indices calculated within (paired *t* tests) and between (independent *t*-tests) patients and normal controls. Sham tumors located at the same positions as real tumors were defined in the cerebellums of normal controls to simulate the paired *t*-tests within the patient group. These sham tumors were also used as the corresponding normal areas in the independent *t*-tests between patients and normal controls as the corresponding normal subjects.

	Paired *t* test within patient group				Paired *t* test within normal controls				Independent *t* test between patients and normal controls			
	Without *Z*-Standardization		With *Z*-Standardization		Without *Z*-Standardization		With *Z*-Standardization		Without *Z*-Standardization		With *Z*-Standardization	
	t	*p*	*t*	*p*	*t*	*p*	*t*	*p*	*t*	*p*	*t*	*p*
ALFF	-3.5230	0.0008	-4.0887	0.0001	1.2988	0.1990	1.3405	0.1852	-2.3933	0.0183	-3.0441	0.0029
fALFF	-2.7400	0.0081	-2.3218	0.0237	0.9123	0.3653	-0.4718	0.6388	-0.3077	0.7588	2.0641	0.0412
ReHo	-1.5875	0.1178	-2.0389	0.0460	-0.8017	0.4259	-1.2470	0.2173	-0.0086	0.9931	1.7137	0.0892
DC	-0.7357	0.4648	-4.9363	6.868×10^{-6}	-1.2062	0.2325	-1.8833	0.0646	-1.2746	0.2049	-0.8370	0.4043
VMHC*	-8.8285	2.21×10^{-12}			-0.8358	0.4069			-5.6797	9.8688×10^{-8}		

* VMHC was not processed with Z-standardization but rather with Fisher's r-to-z transformation, and thus, results of Z-standardization of this metric are not listed

FIGURE LEGENDS

Figure 1. Overlaps of tumors. A total of sixty patients with intracranial tumors located in unilateral posterior cranial fossa, including 23 tumors located on the left side and 37 tumors located on the right side. The tumors overlap probabilistic figures are showed. The stereo cerebellum is presented in the anterior view, and two-dimensional maps are presented in the transverse view.

Figure 2. Common R-fMRI indices of tumors and their corresponding control areas in the patient group and the healthy control group without GSR. ALFF, and fALFF could distinguish tumors from corresponding control regions regardless of whether or not Z-standardization was employed ($p<0.05$). VMHC, which underwent Fisher's r-to-z transformation, also succeeded in detecting tumors. However, ReHo and DC could not detect tumors without Z-standardization ($p>0.05$). Once Z-standardization was employed, all of four indices were able to detect tumors totally (* $p<0.05$, ** $p<0.01$, *** $p<0.001$). Error bars, mean ± s.e.m.

Figure 3. Different profiles of the five R-fMRI indices in detecting tumors. For visualization, we converted the p values to z values to indicate the differences between tumors and control areas. VMHC showed the most significant difference, followed by DC, ALFF, fALFF and ReHo (with Z-standardization). Meanwhile, the significance of the five indices in controls were all higher than 0.05, regardless of whether no not Z-standardization was employed. The green line show *Z* value with $p = 0.05$. The blue line shows *Z* values of each metric calculated using paired *t*-tests without Z-standardization, and the orange line indicates the *Z* values of each metric calculated using paired *t*-tests with Z-standardization (For VMHC, Fisher's r-to-z transformation was performed, and its values are shown on the blue land orange lines).

Figure 4. Common R-fMRI indices of tumors and their corresponding control areas in the patient group and of sham tumors in the healthy control group without GSR. We compared each R-fMRI measure of the tumors with those of the sham tumors in the matched controls, assuming that they had same tumors in same locations, using two samples *t*-test. As the patient tumor and sham tumor came from the different subjects, we were able to investigate a between-subject design. ReHo and DC failed again in distinguishing tumors from corresponding control regions ($p>0.05$), although these metrics demonstrated significant differences

(p<0.05) in the within-subject design. In this analysis, all metrics (except for VMHC, which was compared after Fisher's r-to-z transformation) were calculated with Z-standardization, which is critical for R-fMRI metrics, as shown in Figure 3.

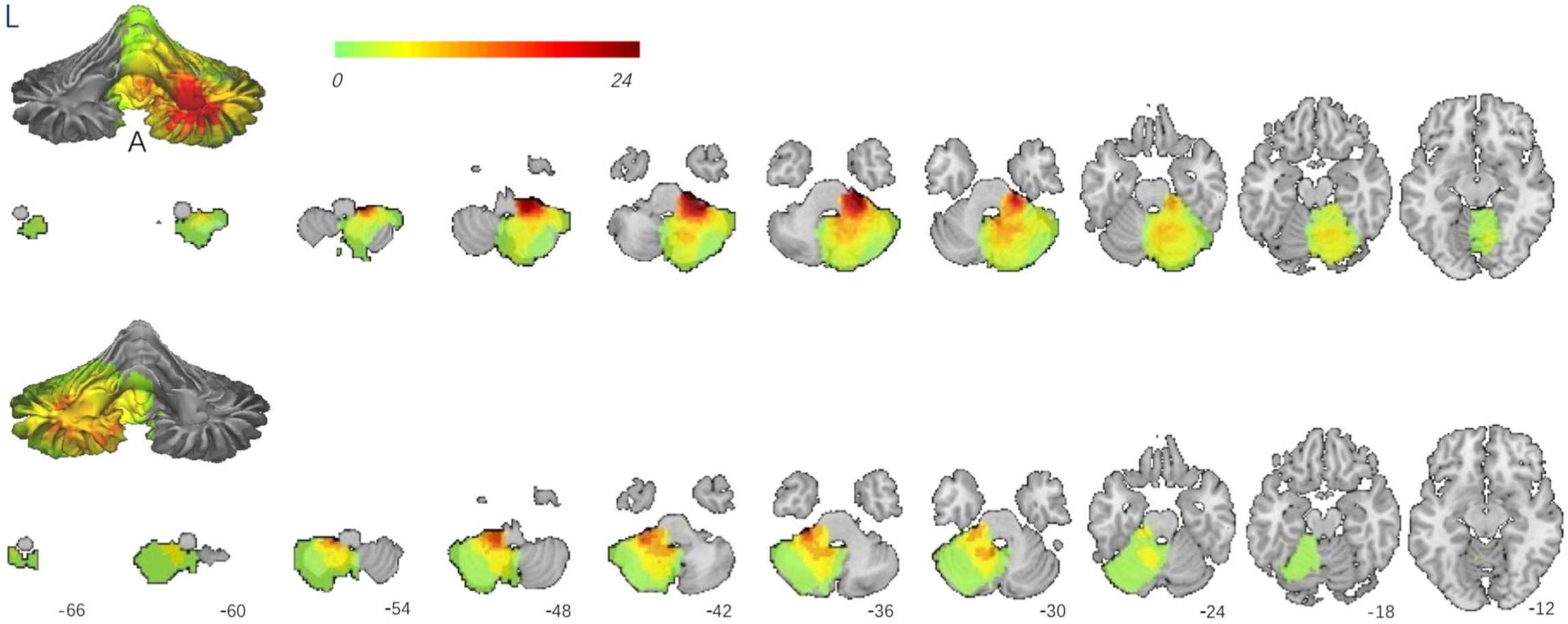
L
A
0
24
-66
-60
-54
-48
-42
-36
-30
-24
-18
-12

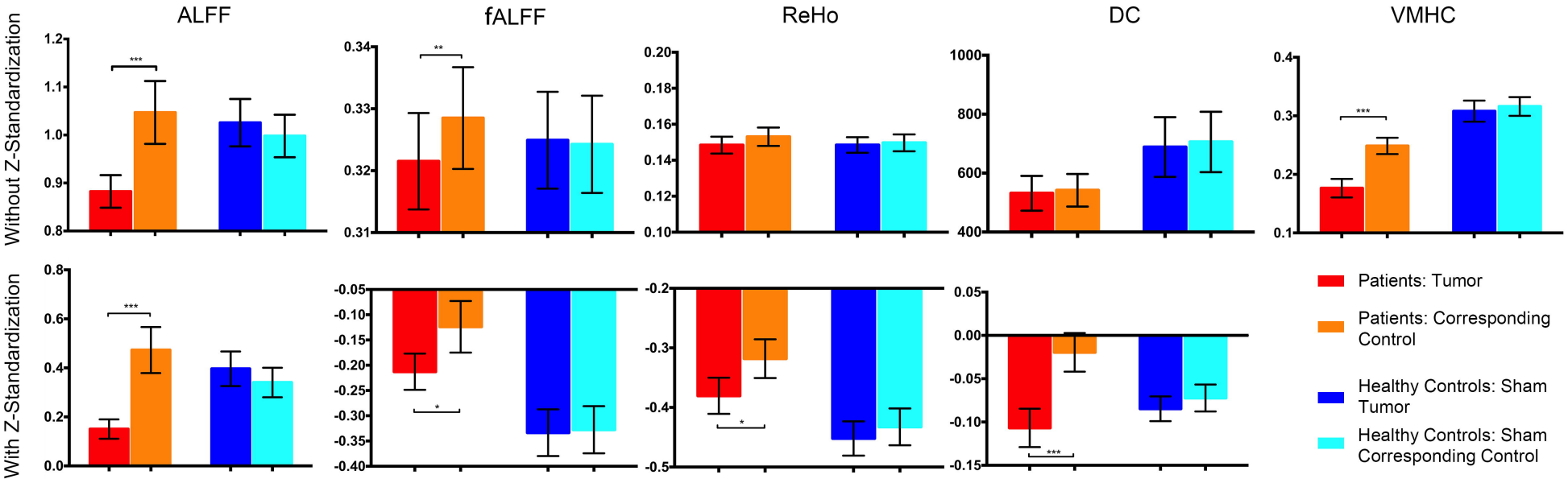
ALFF
fALFF
ReHo
DC
VMHC
Without Z-Standardization
With Z-Standardization
Patients: Tumor
Patients: Corresponding Control
Healthy Controls: Sham Tumor
Healthy Controls: Sham Corresponding Control

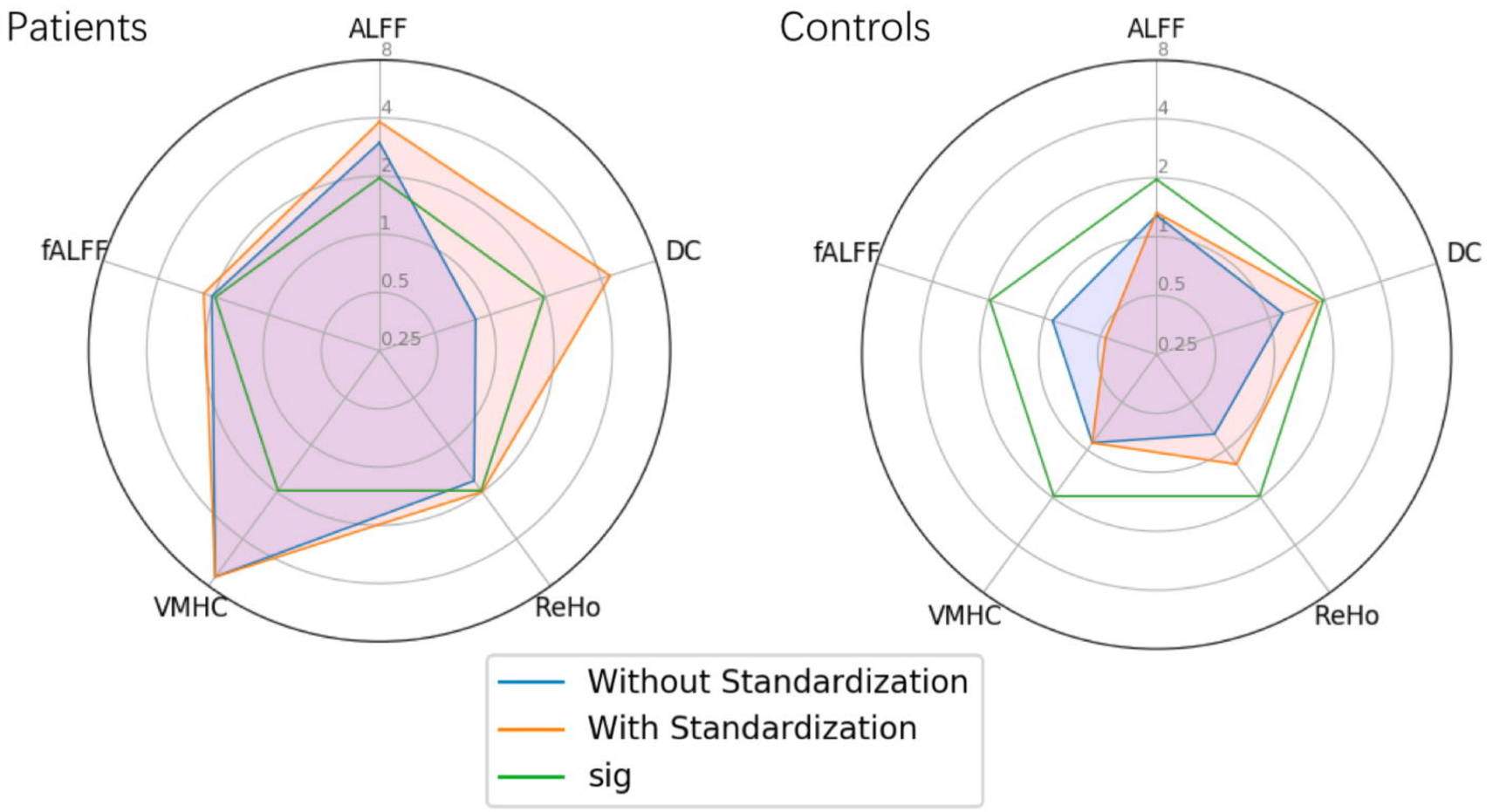
Patients
ALFF
DC
ReHo
VMHC
fALFF
8
4
2
1
0.5
0.25
Controls
ALFF
DC
ReHo
VMHC
fALFF
8
4
2
1
0.5
0.25
Without Standardization
With Standardization
sig

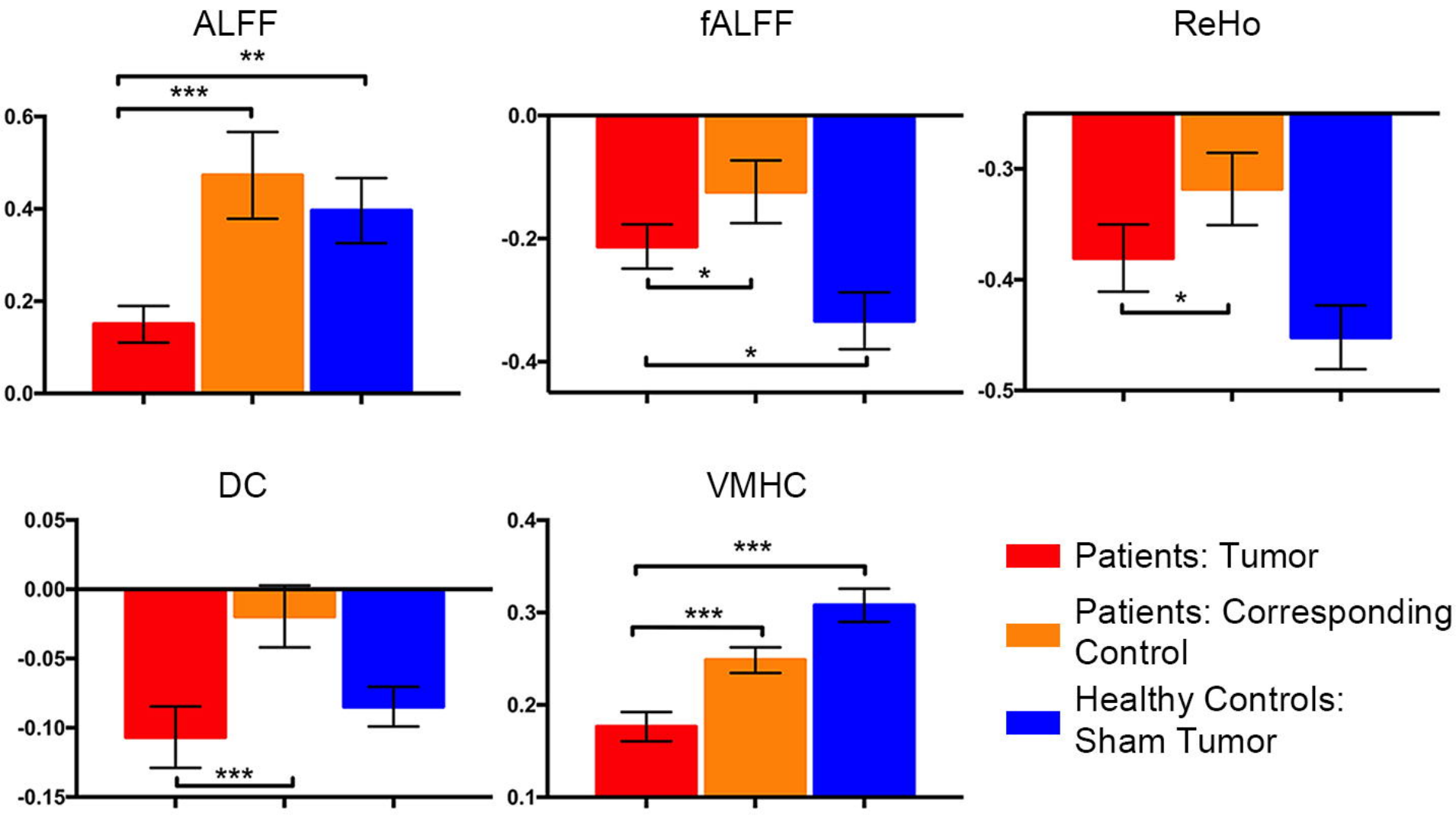
ALFF
**
***
0.6
0.4
0.2
0.0
fALFF
0.0
-0.2
-0.4
*
*
ReHo
-0.3
-0.4
-0.5
*
DC
0.05
0.00
-0.05
-0.10
-0.15
***
VMHC
0.4
0.3
0.2
0.1
***
***
Patients: Tumor
Patients: Corresponding Control
Healthy Controls: Sham Tumor